Super Resolution Convolutional Neural Networks for Increasing Spatial Resolution of 1H Magnetic Resonance Spectroscopic Imaging

Super Resolution Convolutional Neural Networks for Increasing Spatial Resolution of ^{1}H Magnetic Resonance Spectroscopic Imaging

Sevim Cengiz[1] Maria del C. Valdes-Hernandez[2] and Esin Ozturk-Isik[1]

[1] Institute of Biomedical Engineering, Bogazici University, Istanbul, Turkey
sevim.cengiz@boun.edu.tr, esin.ozturk@boun.edu.tr
https://cil.boun.edu.tr
[2] Department of Neuroimaging Sciences Centre for Clinical Brain Sciences University of Edinburgh, Edinburgh, UK
m.valdes-hernan@ed.ac.uk
http://www.ed.ac.uk/clinical-brain-sciences

Abstract. Proton magnetic resonance spectroscopic imaging (^{1}H-MRSI) provides noninvasive information regarding metabolic activity within the tissues. One of the main problems of MRSI is low spatial resolution due to clinical scan time limitations. Advanced post-processsing algorithms, like convolutional neural networks (CNN) might help with generation of super resolution MR spectroscopic images. In this study, the application of super resolution convolutional neural networks (SRCNN) for increasing the MRSI spatial resolution is presented. FLAIR, T1 weighted and T2 weighted MR images were used in training the SRCNN scheme. The spatial resolution of MRSI images were increased by using the model trained with the anatomical MR images. The results of the proposed technique were compared with bicubic resampling in terms of peak signal to noise ratio, structure similarity index, root mean square error, relative polar edge coherence, and visual information fidelity pixel. Our results indicated that SRCNN would contribute to reconstructing higher resolution MRSI.

Keywords: convolutional neural network, super resolution, proton magnetic resonance spectroscopic imaging

1 Introduction

Proton magnetic resonance spectroscopic imaging (^{1}H-MRSI) is commonly used in clinical settings for obtaining information about brain tissue metabolism. Acquisition of ^{1}H-MRSI in addition to standard anotomical MR images, like T1 weighted MRI (T1w MRI), T2 weighted MRI (T2w MRI), and fluid attenuated inversion recovery (FLAIR) MRI, helps in better defining disease characteristics, including multiple sclerosis, brain tumors and Parkinson's disease [1–5]. For instance, studies reported that there was lower N-acetyl aspartate to creatine ratio (NAA/Cr) in occipital lobe of patients diagnosed with Parkinson's disease

with mild cognitive impairment [4, 5], and brain tumors with a mutation in isocitrate dehyrogenase (IDH) have been observed to have higher 2-hydroxyglutarate (2HG) [6–8]. ^{1}H-MRSI detects a number of metabolites present in the tissue in relatively much lower concentrations than water. As a result, higher voxel sizes are employed for ^{1}H-MRSI to increase signal to noise ratio (SNR). Typical ^{1}H-MRS images have a spatial resolution that is 10 times lower than anatomical MR images. A region of 10 by 10 pixels from an anatomical MRI scan shows the tissue imaged in details, whereas the same region often gets represented as a single voxel in ^{1}H-MRSI. Additionally, obtaining high resolution ^{1}H-MRSI would require a long scan time unless scan time reducing imaging strategies are employed [9]. An alternative approach that would result in higher spatial resolution ^{1}H-MRSI without a scan time cost is advanced post-processing methods.

One of such post-processing techniques is convolutional neural network (CNN), which dates back to the 1980s [10]. CNN has been applied in many fields including handwriting [21] or face recognition [20], and object recognition [23] and classification [24]. Additionally, super-resolution CNN (SRCNN) has more recently been proposed to generate higher resolution images out of low resolution versions [11–13]. To our knowledge, SRCNN has not been applied to increase the spatial resolution of anatomical MRI or ^{1}H-MRSI. In this study, we propose to increase the spatial resolution of ^{1}H-MRSI using SRCNN. For this purpose, we present a SRCNN pipeline for post-processing ^{1}H-MRS images using the anatomical information present in T1w, T2w and FLAIR MRI.

2 Materials and Methods

2.1 MR Data Acquisition and Preprocessing

Three healthy subjects, who provided written informed consent before the data acquisition, were included in this study. The imaging experiments were performed on a 3T clinical MR scanner (Philips Medical Systems, Best, Holland) with a 32-channel head coil. For each subject, MRI data acquisition frames were aligned parallel to the anterior commissure (AC) - posterior commissure (PC) line. First, T1w MR (TR/TE=8.3/3.8 ms, FOV=250x250x180 mm, voxel size=1x1x1 mm), T2w MR (TR/TE=10243/80 ms, 90 degree flip angle, FOV= 240x240x180 mm, voxel size=2x2x2 mm), and FLAIR MR (TR/TE=4800/1650 ms, FOV= 250x250x180 mm, voxel size=1x1x3 mm) images were obtained. Afterwards, three dimensional ^{1}H-MRSI data was acquired by using Point-RESolved Spectroscopy (PRESS) sequence (TR/TE=1000/52 ms, FOV=140 mm, voxel size= 10x10x10 mm, 14x14x3 voxels, scan time=8min). T2w MR images were used as the reference images for defining ^{1}H-MRSI region of interests (ROI).

Raw ^{1}H-MRSI data was exported out and the spectra were quantified by using LCModel program [14]. Metabolite concentrations including total N-acetyl aspartate (tNAA) were quantified for each voxel. An in-house software written in MATLAB (The Mathworks Inc., Natick, MA) was used to combine the metabolite concentrations of each voxel into a single tNAA map for each slice.

T1w and FLAIR MR images were rigidly registered to reference T2w MR images using FSL-FIRST [19] so as all anatomical scans were aligned (Figure 1). Additionally, a fused RGB MR image (Fused MRI) was formed by placing T1w, T2w, and FLAIR MR images into three distinct channels of an RGB image using the MCMxxxVI-RGBExplorer tool[3].

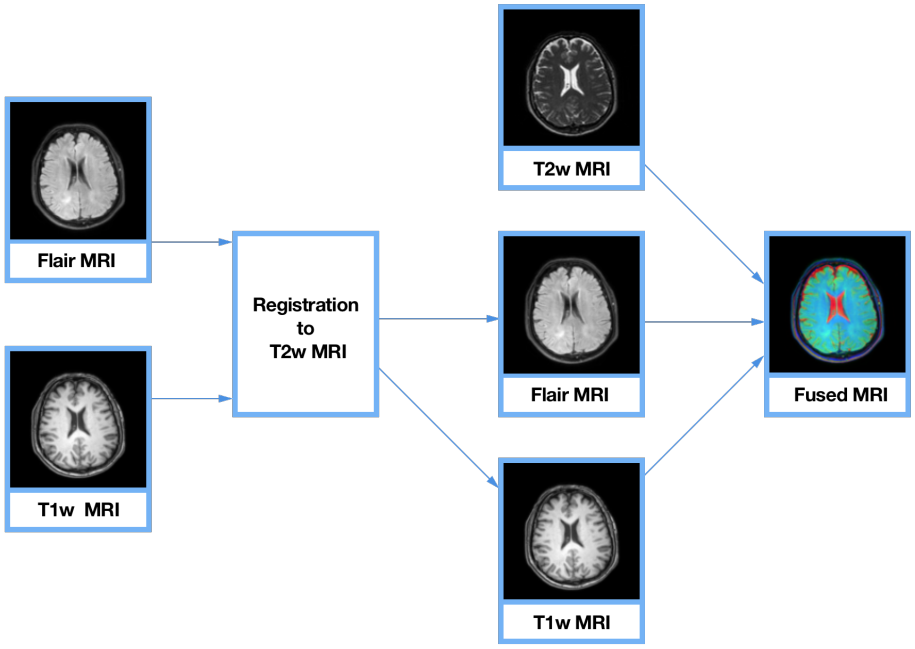

Fig. 1. A schematic of MR image registration and fusion of T1w, T2w, and FLAIR MRI

The spatial resolution of tNAA maps were upscaled by a factor of 1.87 using nearest neighbor interpolation to match the T2w MR image resolution. T1w, T2w, and FLAIR, and Fused MR image regions that have the same spatial coordinates with the tNAA maps were extracted (Figure 2).

2.2 SRCNN Post-Processing

Caffe [15] was installed as a deep learning framework for SRCNN to train super-resolution models. SRCNN structure included three convolutional layers. The weight filler type was set as Gaussian, base learning rate was set as 0.0001, and the learning policy was fixed. As per the training/testing strategy from

[3] https://sourceforge.net/projects/bric1936/files/MATLAB/

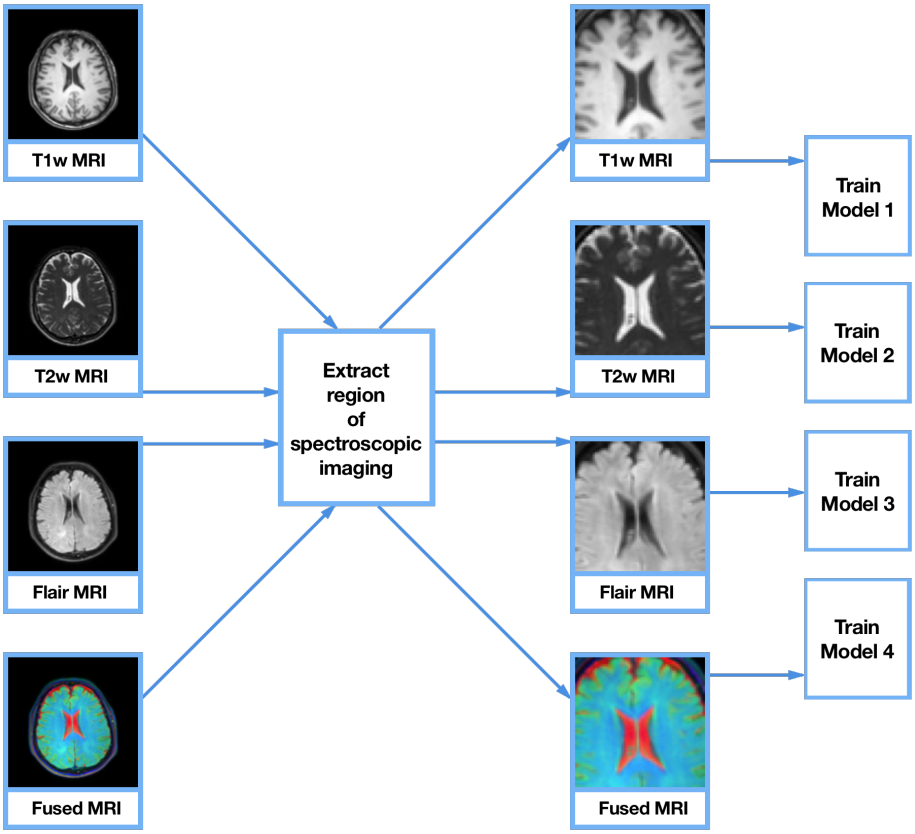

Fig. 2. A schematic pipeline of ROI extraction and training of anatomical MRI

[22], the extracted regions of the structural MR images and Fused MRI were downsampled and fed into the SRCNN to train four separate models (Figure 2). tNAA maps were used as the testing dataset, and the four distinct models trained on different structural MR images or Fused MRI were employed in SRCNN to upscale the spatial resolution of tNAA maps by a factor of three. Three iteration levels, which were 10.000, 100.000, and 1.000.000 iterations, were employed to determine the number of necessary iterations for good spatial resolution. The results of the SRCNN were compared with bicubic interpolation.

2.3 Image Quality Evaluation Metrics

Peak to noise ratio (PSNR), root mean square error (RMSE), structural similarity index (SSIM) [16], relative polar edge coherence (RECO)[18], and visual information fidelity pixel (VIFP) [17] were used as evaluation metrics of accuracy on all experiments in our study. The tNAA map that was upsampled by nearest neighbor interpolation was used as the reference image for comparison purposes.

3 Results

SRCNN was first applied to increase the spatial resolution of anatomical and fused MR images by using the corresponding image for both train and test datasets. SRCNN resulted in higher mean PSNR, and lower RMSE than bicubic interpolation for all anatomical MR datasets and fused MRI after 10.000 iterations (Table 1). When T2w MRI and Fused MRI were used as SRCNN training datasets, 10.000 iterations was not sufficient to outperform bicubic interpolation. For T1w MRI and FLAIR MRI, highest mean PSNR and lowest RMSE values were obtained when 100.000 iterations were used for SRCNN.

Table 1. The mean PSNR and RMSE of anatomical MRI and Fused MRI datasets

		T1w MRI		**T2w MRI**		**FLAIR MRI**		**Fused MRI**	
Method	**# Iteration**	**PSNR**	**RMSE**	**PSNR**	**RMSE**	**PSNR**	**RMSE**	**PSNR**	**RMSE**
Bicubic SR	-	25.11	14.14	25.11	14.14	27.23	11.09	31.56	6.73
SRCNN	10000	25.21	13.98	24.81	14.64	27.52	10.71	30.67	7.46
SRCNN	100000	25.86	12.98	25.92	12.89	28.13	9.99	32.11	6.32
SRCNN	1000000	25.85	13	26.1	12.63	27.77	10.42	32.36	6.2

Four distinct training models obtained from SRCNN algorithm based on different anatomical or Fused MRI were applied to tNAA maps to get higher spatial resolution. Table 2 displays the PSNR and RMSE values when bicubic interpolation or SRCNN with varying number of iterations were employed for super-resolution ^{1}H-MRSI. T1w MRI model did not result in higher PSNR or lower RMSE than bicubic interpolation. FLAIR MRI and Fused MRI models with 100.000 and 1.000.000 iterations, respectively, resulted in highest PSNR

and lowest RMSE with good image contrast. Figure 3 shows our SRCNN results for increasing ^{1}H-MRSI spatial resolution. According to the results, tNAA maps upscaled by a factor of 3 using Fused MRI filter model with 100.000 iterations qualitatively had the best image contrast. The worst image definition was observed in tNAA maps using T2w MRI filter model.

Table 2. The mean PSNR and RMSE results of SRCNN for super-resolution MRSI based on different anatomical MRI training models

		T1w MRI		**T2w MRI**		**FLAIR MRI**		**Fused MRI**	
Method	**# Iteration**	**PSNR**	**RMSE**	**PSNR**	**RMSE**	**PSNR**	**RMSE**	**PSNR**	**RMSE**
Bicubic SR	-	27.01	11.37	27.01	11.37	27.01	11.37	27.01	11.37
SRCNN	10000	26	12.77	23.47	17.09	27.05	11.32	24.015	16.06
SRCNN	100000	26.69	11.79	27.88	10.28	27.58	10.64	27.77	10.41
SRCNN	1000000	25.94	12.86	26.08	12.65	26.29	12.35	28.17	9.95

Figure 4 shows PSNR, RMSE, SSIM, RECO, and VIPF image metric results of bicubic resampling (starting point) versus SRCNN (endpoint) for increasing spatial resolution of MRSI using models trained on T1w MRI, T2w MRI, Flair MRI, and Fused MRI. SRCNN training resulted in a higher RECO and a lower RMSE value than bicubic interpolation. SSIM, PSNR, and VIFP values were slightly smaller for SRCNN than bicubic resampling.

4 Conclusion and Discussion

In this paper, we have presented a novel application of SRCNN deep learning method for increasing spatial resolution of ^{1}H-MRSI based on the anatomical image definition of T1w, T2w and Flair MRI, and their Fused MR images. We have used tNAA maps as an example spectral image in this study. Our results could be similarly applied to increase the spatial resolution of other metabolite maps that could be obtained by ^{1}H-MRSI. The proposed approach may contribute to clinical 3D ^{1}H-MRSI applications. Future studies will be conducted to investigate the use of other deep learning methods, like fast SRCNN (FSRCNN) and patch-based super-resolution, to increase the spatial resolution of MR spectroscopic metabolite maps.

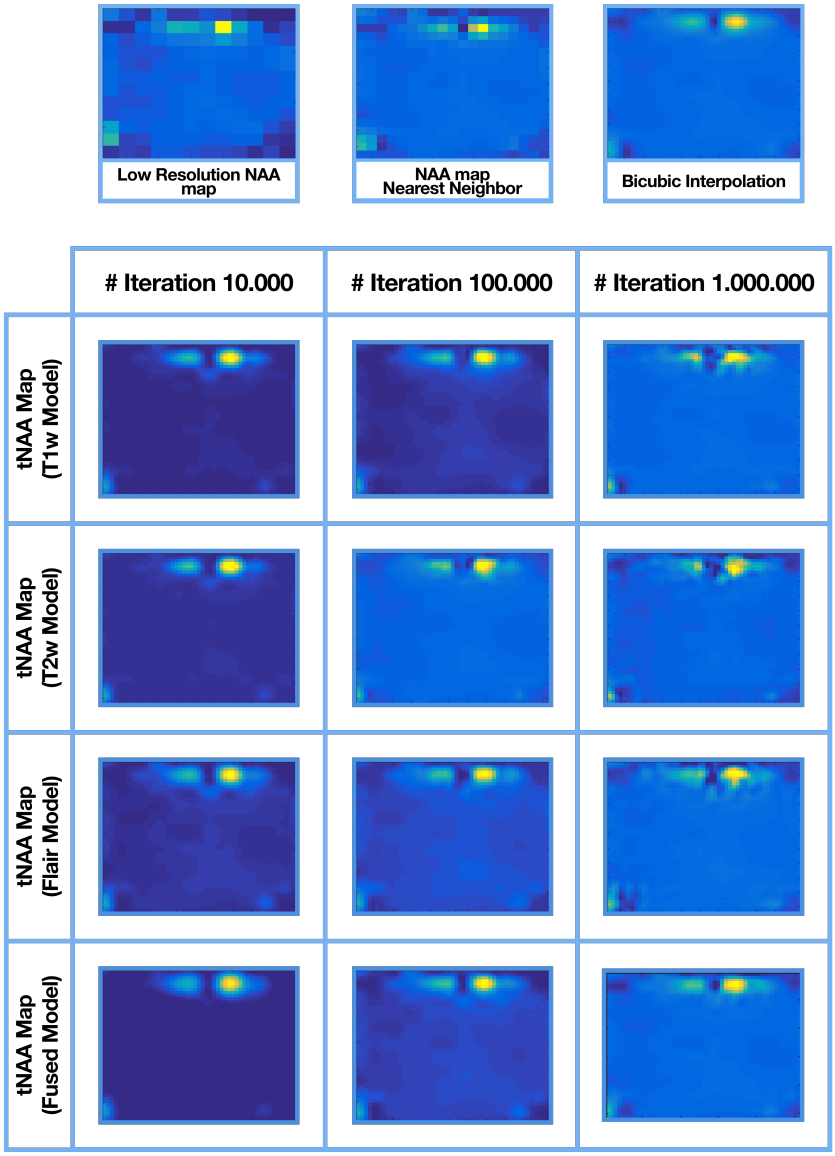

Fig. 3. SRCNN results of an example tNAA map upscaled by using T1w, T2w, FLAIR, and Fused MRI filter models with 10.000, 100.000, and 1.000.000 iterations

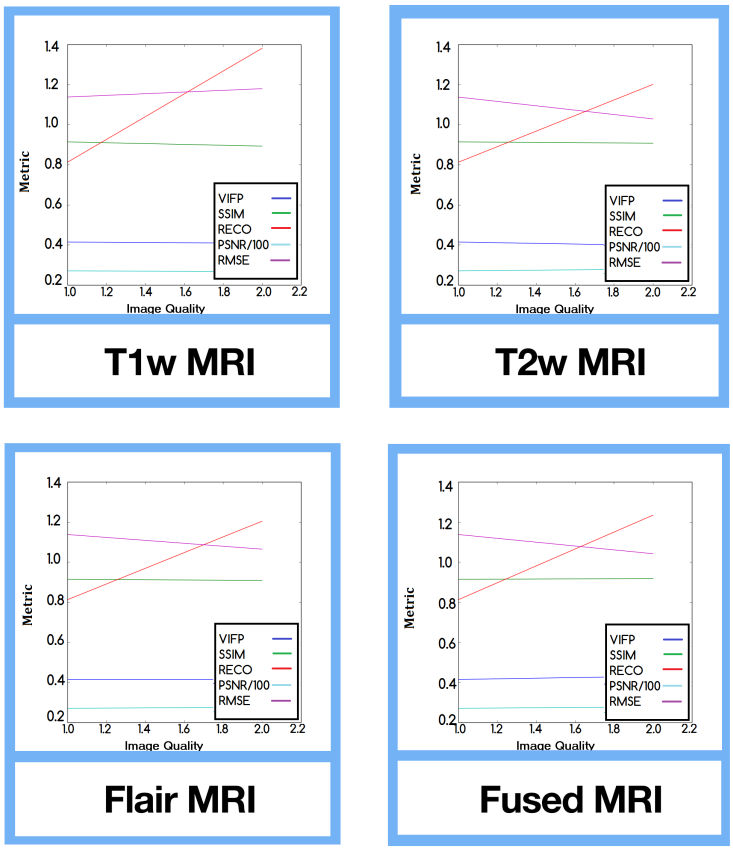

Fig. 4. Image quality metric results for increasing MRSI spatial resolution using bicubic interpolation (starting point) or SRCNN models (end point) trained on T1w MRI, T2w MRI, Flair MRI, and Fused MRI.

References

1. Nelson, S. J.: Multivoxel magnetic resonance spectroscopy of brain tumors. Mol Cancer Ther 2, 497-507 (2003)
2. Filippi, M., and Agosta, F.: Imaging biomarkers in multiple sclerosis. J. Magnet. Reson. Imaging 31, 770788 (2010)
3. Rovira, A., Auger, C., and Alonso, J.: Magnetic resonance monitoring of lesion evolution in multiple sclerosis. Therapeut. Adv. Neurol. Disord. 6, 298310 (2013)
4. Camicioli, R. M., Korzan, J. R., Foster, S. L., Fisher, N. J., Emery, D. J., Emery, A. C., and Hanstock, C. C.: Posterior cingulate metabolic changes occur in parkinsons disease patients without dementia. Neurosci Lett, Vol. 354, no. 3, pp. 17780 (2004)
5. Griffith, H. R., Hollander, J. A., Okonkwo, OBrien, O. C., T., Watts, R. L., and Marson, D. C.: Brain n-acetylaspartate is reduced in parkinson disease with dementia. Alzheimer Dis Assoc Disord, Vol. 22, no. 1, pp. 5460 (2008)
6. Andronesi, O. C., Kim, G. S., Gerstner, E., Batchelor, T., Tzika, A. A., Fantin, V. R., Vander Heiden, M. G., and Sorensen, A. G.: Detection of 2-hydroxyglutarate in idh-mutated glioma patients by in vivo spectral-editing and 2d correlation magnetic resonance spectroscopy. Sci Transl Med, 4(116):116ra4 (2012)
7. Elkhaled, A., Jalbert, L. E., Phillips, J. J., Yoshihara, H. A., Parvataneni, R., Srinivasan, R., Bourne, G., Berger, M. S., Chang, S. M., Cha, S., and Nelson, S. J.: Magnetic resonance of 2-hydroxyglutarate in idh1-mutated low-grade gliomas. Sci Transl Med, 4(116):116ra5 (2012)
8. Choi, C., Ganji, S. K., DeBerardinis, R. J., Hatanpaa, K. J., Rakheja, D., Kovacs, Z., Yang, X. L., Mashimo, T., Raisanen, J. M., Marin-Valencia, Pascual, I. J., Madden, M. C., Mickey, J. B. E., Malloy, C. R., Bachoo, R. M., and Maher, E. A.: 2-hydroxyglutarate detection by magnetic resonance spectroscopy in idh-mutated patients with gliomas. Nat Med, 18(4):6249 (2012)
9. Nelson SJ, Ozhinsky E, Li Y, Park I, Crane J. Strategies for rapid in vivo 1H and hyperpolarized 13C MR spectroscopic imaging. J Magn Reson 2013; 229:187-197.
10. Le Cun, Y., Boser, B., Denker, J. S., Henderson, D., Howard, R. E., Hubbard, W., and Jackel, L. D.: Backpropagation applied to hand- written zip code recognition. Neural Comput., vol. 1, no. 4, pp. 541551 (1989)
11. Saurabh, J., Diana, M. S., Faezeh, S. N., Gilbert, H., Wolfgang, B., Stephen, W., Sabine, V. H., Frederik Dirk, M. S.: Patch-Based Super-Resolution of MR Spectroscopic Images: Application to Multiple Sclerosis. Frontiers in Neuroscience 11(13) (2017)
12. Dong, C., Loy, C. C., He, K., and Tang, X.: Image super- resolution using deep convolutional networks. IEEE Trans. Pat- tern Anal. Mach. Intell., vol. 38, no. 2, pp. 295307 (2016) doi: 10.1109/TPAMI.2015.2439281.
13. Kim, J., Lee, J. K. and Lee, K. M.: Accurate image super-resolution using very deep convolutional networks. In Proc. IEEE Conf. Comput. Vis. Pattern Recognit (2016)
14. Provencher, S. W.: Automatic quantitation of localized in vivo 1h spectra with lcmodel, NMR Biomed, Vol. 14, no. 4, pp. 2604 (2001)
15. Jia, Y., Shelhamer, E., Donahue, J., Karayev, S., Long, J., Girshick, R., Guadarrama, S., and Darrell, T.: Caffe: Convolutional Architecture for Fast Feature Embedding. ArXiv preprint arXiv:1408.5093 (2014)
16. Wang, Z., Bovik, A. C., Sheikh, H. R., and Simoncelli, E. P.: Image quality assessment: From error measurement to structural similarity. IEEE Trans. Image Process., vol. 13, no. 4, pp. 600612 (2004)

17. Sheikh, H. R., and Bovik, A. C.: Image information and visual quality. Image Processing, IEEE Transactions on, vol. 15, no. 2, pp. 430444 (2006)
18. Baroncini, V., Capodiferro, L., Di Claudio, E. D., and Jacovitti, G.: The polar edge coherence: a quasi blind metric for video quality assessment. EUSIPCO 2009, Glasgow, pp. 564568 (2009)
19. Smith, S.M., Jenkinson, M., Woolrich, M.W., Beckmann, C.F., Behrens, T.E.J., Johansen-Berg, H., Bannister, P.R., De Luca, M., Drobnjak, I., Flitney, D.E., Niazy, R., Saunders, J., Vickers, J., Zhang, Y., De Stefano, N., Brady, J.M., and Matthews, P.M.: Advances in functional and structural MR image analysis and implementation as FSL. NeuroImage, 23(S1):208-19 (2004)
20. Lawrence, S., Giles, C. L., Tsoi, A. C., Back, A. D. Face recognition: a convolutional neural-network approach. IEEE Transactions on Neural Networks. 8(1):98113 (1997)
21. Pang, S, Yang, X.: Deep Convolutional Extreme Learning Machine and Its Application in Handwritten Digit Classification. Comput Intell Neurosci. 2016;2016:3049632. doi: 10.1155/2016/3049632 (2016)
22. Valdes, M.DelC., Inamura, M.: Improvement of remotely sensed low spatial resolution images by back-propagated neural networks using data fusion techniques. International journal of remote sensing, 22(4):629-642 (2001)
23. Xu, Z., Cheng, X. E.: Zebrafish tracking using convolutional neural networks. Scientific Reports, 7, 42815 (2017)
24. Pang, S., Yu, Z., Orgun, M.A.: A novel end-to-end classifier using domain transferred deep convolutional neural networks for biomedical images. Comput Methods Programs Biomed. 2017 Mar;140:283-293. doi: 10.1016/j.cmpb.2016.12.019 (2017)